Preliminary Characterization Results of the Optical Communications Telescope Laboratory Telescope

K. Wilson,[1] A. Vaughan,[2] J. Wu,[1] D. Mayes,[3] J. Maloney,[4] and R. Sobek[4]

NASA has identified deep-space optical communications as one of the key technologies to enable rapid data return from high-data-rate science instruments on probes exploring the solar system. The JPL Optical Communications Telescope Laboratory (OCTL) telescope was built by Brashear and is a research and development instrument for exploring several of the challenges associated with the deployment and operation of an optical transceiver facility for deep-space optical communications. The telescope is designed to track objects from deep space down to a 250-km altitude with a 6-deg key hole—an excluded tracking zone near zenith. Its magnitude is a function of the target satellite's altitude. It consists of a 1-m F/75.8 main telescope with a 500-μrad field of view and a 0.2-m acquisition telescope having a 5.24-mrad (0.3 deg) field of view. Among the key requirements of the OCTL telescope are (1) operation down to 10 deg of the sun, (2) blind pointing to better than 3 arcseconds after mount calibration, and (3) tracking a target under 50-km/h wind loading. Designed as a communications instrument for the near-infrared 1064-nm and 1550-nm wavelengths, the telescope coatings are highly reflective over the range from 500 nm to 2000 nm. The measured residual wave-front error of the telescope as installed is λ/7 root-mean-square at 633 nm.

I. Introduction

The JPL 1-m research and development (R&D) Optical Communications Telescope Laboratory (OCTL) telescope was installed at JPL's Table Mountain Facility (TMF) on July 26, 2003. Key characteristics of the telescope presented in this article are (1) the residual wave-front error of the as-mounted telescope, (2) the tracking performance of the telescope with and without wind loading, and (3) the blind pointing accuracy of the telescope.

---

[1] Communications Architectures and Research Section.

[2] Space Experiments Systems Section, JPL retiree contracted through Chipton-Ross, Inc., El Segundo, California.

[3] Earth Sciences Section.

[4] Brashear L3-Communications, Pittsburgh, Pennsylvania.

The research described in this publication was carried out by the Jet Propulsion Laboratory, California Institute of Technology, under a contract with the National Aeronautics and Space Administration.

The statement of work for the telescope procurement specified the performance requirements of the telescope. This is the first of a series of articles in which we describe the results of the telescope characterization tests. In this article, we discuss the factory acceptance test results and the results of preliminary tests made at the OCTL. Initial tests of the telescope as delivered in July 2003 showed significant astigmatism. Investigation revealed that the primary mirror had shifted in its cell. This was attributed to jarring of the primary in its mount during the cross-country shipment. The primary and cell were returned to the vendor for repair in September 2003. The repaired system was reinstalled in November 2003. The work at the OCTL facility reported on here describes the performance of the telescope after November 2003. These data are the preliminary results taken over the period from January 2004 to August 2004 and prior to the formal site acceptance tests of the telescope. As of this article, the Sun-avoidance algorithm is the only remaining software algorithm to be completed before site acceptance test. Because Sun avoidance was not operational, daytime seeing measurements were made using only the star Polaris, which was consistently greater than 30 deg from the Sun.

In Section II, we present the key performance requirements of the telescope. Where applicable, we describe the method of testing and validation of these requirements. Some measurements were made at the vendor's facility in Pittsburgh and others, such as the mirror coatings, were made at the subcontractor, Denton Vacuum. In Section III, we describe the OCTL environment, i.e., the atmospheric conditions at TMF during the on-site tests. We present the results of the mirror-coating tests and the Hartmann tests in Section IV. The Hartmann approach minimizes the contributions of atmospheric tip/tilt and other atmospheric aberrations from the measurement, and the measured ($\lambda/7$) wave-front error is representative of the residual wave-front error in the optical train. In Section V, we describe the gimbal jitter measurements made with the dome open and closed. Early blind pointing results are presented in Section VI. Subsequent blind pointing measurements made with the radar system and long-wave infrared camera mounted on the telescope showed degraded telescope performance. Subsequent tests showed that the telescope was in an unbalanced condition during these measurements. The requisite counterweights have been fabricated, and these measurements will be repeated and reported along with the tracking performance measurements after the telescope is rebalanced and tuned.

II. Performance Requirements of the OCTL Telescope

The JPL OCTL telescope specification document contains 135 distinct requirements that the vendor Brashear had to validate. Of these, 37 were identified for formal site acceptance testing. The remaining specifications were verified either through tests performed at the factory (optical wave front, controller operations, and hardware verification) or a sub-contractor's facility (Denton Vacuum for mirror coatings), or through analysis. Table 1 lists the specified and measured performances of the key optical elements in the telescope. The gimbal jitter specifications and performance are discussed in Section V. The telescope specification also calls for supporting a variety of distinct pointing formats, described in Section VI. The performance of mechanical components, such as the telescope secondary motion and primary cell cover, etc., are continuously validated as the telescope is used and are not discussed here.

III. The OCTL Environment

Site acceptance tests will be conducted at the OCTL telescope located on Table Mountain in the San Gabriel mountain range 2.2-km above sea level. The climate is mostly arid with winter and snow fall extending from November through April. Atmospheric seeing and cloud cover are of particular interest in assessing potential sites for an optical communications facility. Atmospheric seeing is defined as the blurring of the image of a point source at zenith by atmospheric turbulence. It is defined at the 500-nm wavelength as full-width at half-maximum (FWHM) of the signal integrated over a period of seconds. It varies with wind speed, temperature, and altitude.

Table 1. Telescope performance requirements and results from preliminary acceptance tests.

Number	Item	Specification/ design	Measured	Where measurement was made
		Main telescope		
1	Primary aperture	1.0	1.00 (+0.05 − 0)	Factory
2	Secondary obscuration	<10%	9.81%	Factory
3	Focal length, m	75.79995	75.80909	Factory
4	Field of view, rad	500×10^{-6}	TBD	OCTL
5	Wave-front error, waves at 632-nm	0.054 —	0.063 0.14	Factory OCTL
6	% Encircled energy in Airy disk	>65%	70.8	Factory
7	% Encircled energy in first ring	>80%	86	Factory
8	Azimuth travel limit	±200 deg	±335 deg	Factory
9	Elevation travel limit	−5 deg to +185 deg	−5 deg to +185 deg	Factory
10	Maximum azimuth speed	20 deg/s	25 deg/s	Factory
11	Maximum elevation speed	5 deg/s	10 deg/s	Factory
12	Location of coudé focus	2.1 m from M7	2.1 m from M7	Factory and verified at OCTL
13	Reflectance of M1–M7 mirrors 2000 nm > λ > 600 nm	>98%	>98%	Denton Vacuum
14	Operating temperature range	−10 deg C < T < +40 deg C	TBD	OCTL
15	Peak power damage threshold in 10-ns pulse	10 mJ/cm^2	TBD	OCTL
16	Average power damage threshold	100 W/cm^2	TBD	OCTL
17	Wind conditions	0 < v < 50 km/h (gusts)	<25 km/h	OCTL
18	Relative humidity	0% < RH < 80%	0% < RH< 80%	OCTL
19	Sun avoidance	Operator-specified avoidance cone >10 deg	TBD	OCTL
20	Key hole for 250-km satellite track	6 deg	6 deg	OCTL
		Acquisition telescope		
21	Aperture, cm	20	20	Factory
22	Field of view, rad	5.1×10^{-3}	—	—
23	rms wave-front error, waves at 632 nm	0.07	0.05 ± 0.004	Factory
24	% encircled energy in Airy disk	68	68.1 ± 1.74	Factory
25	Focus control	Automatic	Automatic	OCTL

Figure 1 shows recent data from the OCTL at the Table Mountain Facility taken through an 810-nm interference filter. The measurements, images of the star Polaris, were made with an Apogee AP47p cooled charge-coupled device (CCD) camera over the period from March through June 2004 and are both daytime and nighttime measurements.[5] The 810-nm filter used to provide contrast of the star image against the sky background in the day also was used for nighttime measurements. The data in Fig. 1 have been corrected to 500 nm using Eq. (1) and compensated for the air mass at the 55-deg zenith angle of Polaris as seen from the OCTL, using the relationship in Eq. (2):

$$\theta_1 = \theta_2 \left(\frac{\lambda_2}{\lambda_1} \right)^{1/5} \tag{1}$$

$$\theta(\xi) = \theta_0 \sec^{3/5}(\xi) \tag{2}$$

The results show that the seeing ranged from 4 μrad to 23 μrad.[6] It should be noted that the seeing is not very different from that observed during the 1995 and 1996 laser communications experiments with the ETS-VI satellite [1].

The pointing and tracking performance of the telescope is affected by the wind. A measure of the wind speeds over the three-month period from June 2004 to August 2004 (Table 2) shows that wind speeds were less than 15 km/h for more than 85 percent of the time and less than 30 km/h for approximately 99 percent of the time. Figure 2 shows that for the month of July the winds are highest in the late afternoon and early evening and lowest around sunrise.

Figure 3 shows that the prevailing wind direction at TMF is from the southwest. This is confirmed visually from the northeasterly pointing direction of the pine tree branches at the mountain.

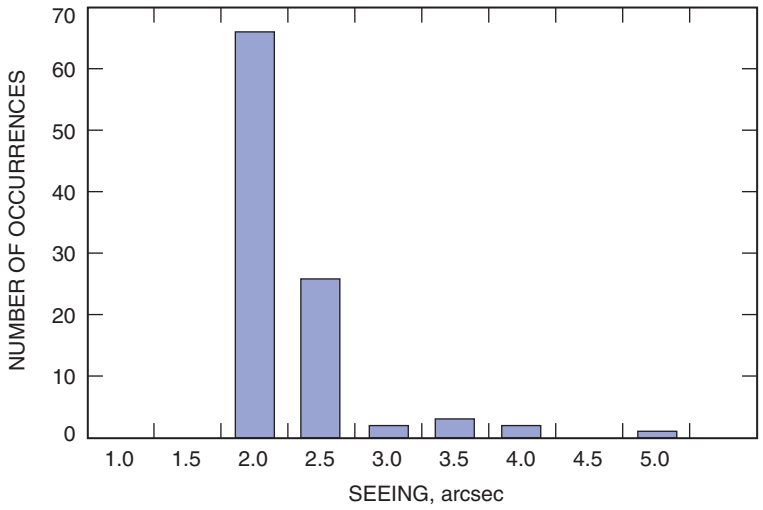

Fig. 1. Histogram of atmospheric seeing at the OCTL for the months March, April, and June 2004. Measurements were made using Polaris and include both daytime and nighttime measurements. The data are corrected for zenith angle and wavelength.

[5] D. Mayes, "TMF Seeing Statistics," JPL Interoffice Memorandum (internal document), Jet Propulsion Laboratory, Pasadena, California, 2004.

[6] Ibid.

Table 2. Distribution of wind speeds at TMF during the Months of June, July, and August.

UT month	Wind speed probabilities, percent		
	$0 = WS < 15$ km/h	$15 = WS < 30$ km/h	$WS = 30$ km/h
June 2004	92	8	<1
July 2004	84	15	1
August 2004	86	13	<1

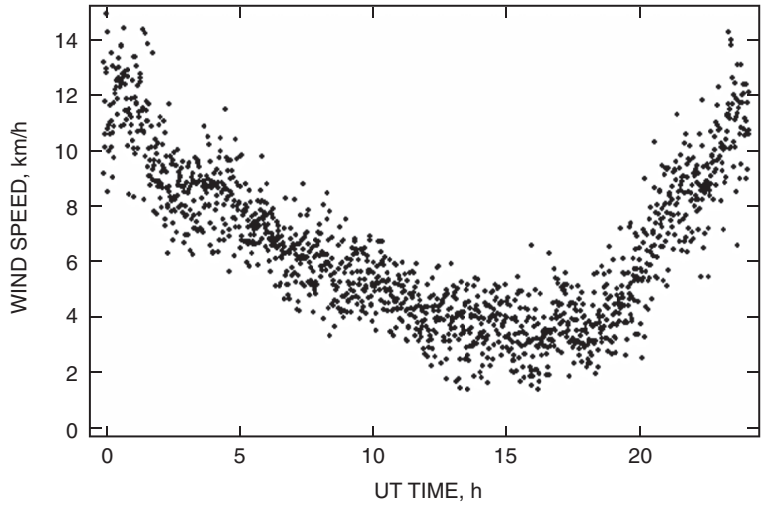

Fig. 2. Temporal variation in mean wind speed values for July 2004.

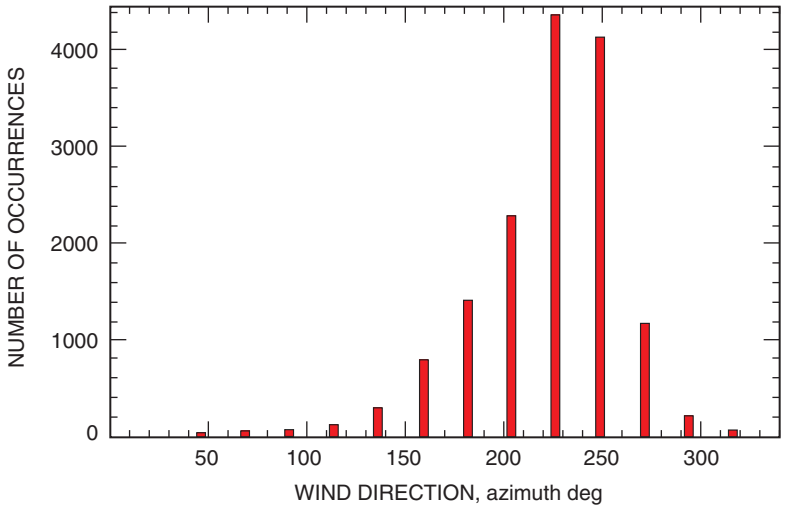

Fig. 3. Wind direction azimuth angle histogram plot for July 2004.

IV. Main Telescope Optics

The main telescope consists of a 1-m parabolic primary f#1.5 and a hyperbolic secondary. In addition, there are five flat turning mirrors that relay images to the coudé room. The M3 and M4 mirrors sit along the elevation axis, and the M6 and M7 along the azimuth axis. An f/78.5 focal system, the focus of the telescope extends approximately 2 m from the M7 mirror into the insulated coudé room. Optical flats designed for maximum transmission at the 532-nm, the 81-nm, and the 1064-nm wavelengths are installed in a tube between the M6 and M7 mirrors to maintain separate thermal environments of the dome and coudé room. Air is continuously blown across the flats to keep them clean and to circulate the air in the tube on both sides of the flats

A. Mirror Coating

The seven mirrors in the telescope coudé path are covered with a protected Denton FSS-99 (Front Surface Silver-99) coating. The specified requirement of greater than 98 percent reflectivity over the 600-nm to 2000-nm wavelength band corresponds to greater than 85 percent throughput to the focal plane for the newly coated surfaces shown in Fig. 4. The dielectric coating is designed to extend the life of the silver coating in the arid southwest climate, and it is specified to withstand peak laser power densities of 10 mJ/cm^2 in a 10-ns pulse, and average power densities of 100 W/cm^2.

B. Telescope Optical Wave Front

The wave-front error of the reassembled telescope was measured at the OCTL and was made using the Hartmann mask technique. The procedure is described in detail in [2]. The mask (Fig. 5), consisting of 20 evenly spaced holes of 10-cm diameter in a rectangular array, was placed in front of the 1-m telescope aperture. A CCD array detector was placed at a known distance (about 0.64 to 0.97 meter) outside the paraxial coudé focus of the telescope. Light from a star passing through the mask thus

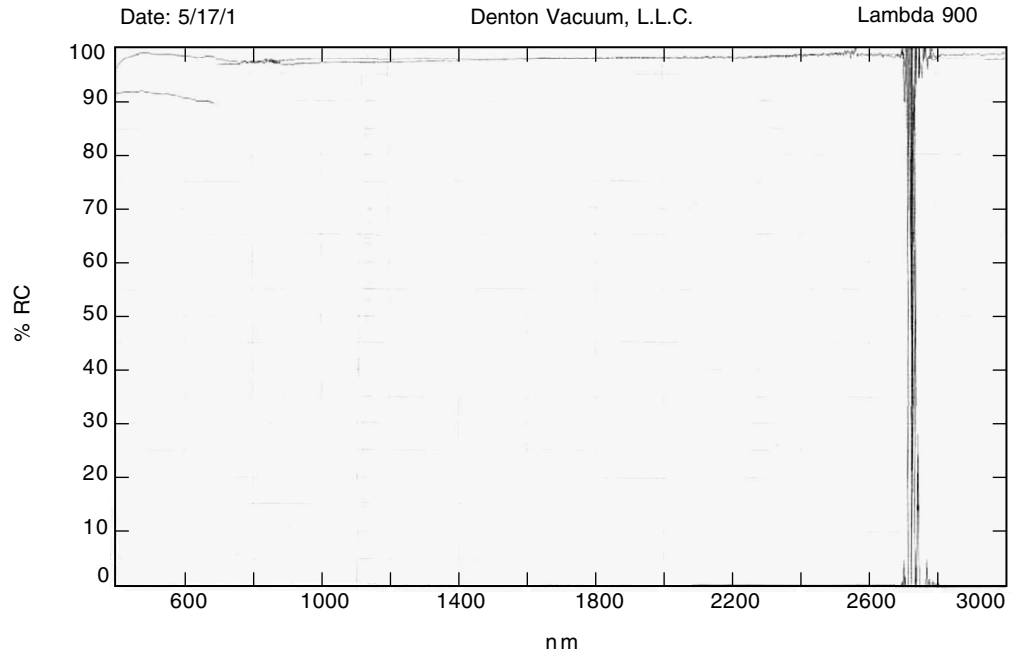

Fig. 4. Reflectivity test results of FSS-99-protected silver witness sample showing greater than 98 percent reflectivity over the 600-nm to 2000-nm wavelength band. (Redrawn from a Brashear Systems LP drawing.)

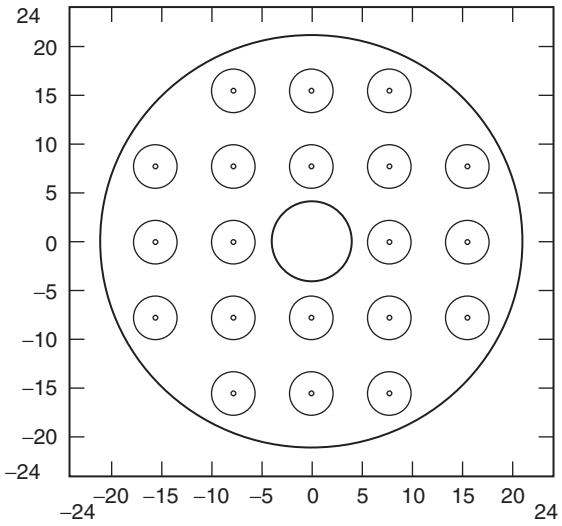

Fig. 5. Schematic of the Hartman mask used for wave-front measurement, showing the relative positions of holes.

created 20 approximately evenly spaced images (blur spots) on the detector. The measured centroids of these images (compared to the ray intercepts for a perfect optical system predicted by ray tracing) served to measure the wave-front slope errors at the corresponding locations on the entrance pupil of the telescope. The slope errors thus measured were fitted (by a least-squares procedure) to the x- and y-derivatives of low-order Zernike polynomials serving to represent wave-front errors corresponding to tilt, defocus, astigmatism, and coma. The estimated root-mean-square (rms) wave-front measuring errors associated with this process (allowing for averaging of the effects of atmospheric turbulence over multiple 60-second exposures and considering possible systematic errors arising from mask fabrication errors) are approximately 0.01 wave HeNe.

Table 3 gives the measured wave-front error from a total of twenty-three 60-second exposures taken at two positions (0.97 m and 0.64 m) from focus. See Figs. 6(a) and (b).

V. Gimbal Jitter Characterization

The jitter described here is the mechanical vibration of the telescope structure as measured at different points. It is not the optical line-of-sight jitter. The telescope specification called for the mechanical rather than the optical line-of-sight jitter. Results of measurements of the optical line-of-sight jitter using a star would represent a combination of contributions from the atmosphere and the vibrations of the telescope structure. For typical seeing conditions and telescope vibration responses, such a measurement would have provided no clear path to identify the source of any variances from the specifications.

We define jitter as the time-varying position difference between the commanded pointing position and the actual pointing position of the telescope. Because jitter is a response to near-random disturbances to the pointing-control system, it is identified as rms. For stiff structures, the gimbal jitter (measured on the trunion box near the primary mirror) is a reasonable approximation to the optical line-of-sight jitter. The main sources for gimbal jitter are tabulated in a statistical error budget as shown in Fig. 7.

The gimbal jitter originates from various sources with identifiable frequency characteristics. The sensor noise is broadband. Drive errors are low frequency. The wind is concentrated at frequencies below 10 Hz,

Table 3. Measured wave-front error using the Hartmann mask.

Aberration	Series 1, waves 633 nm	Series 2, waves 633 nm	Both series, waves 633 nm
X-astigmatism	$+0.11 \pm -0.02$	$+0.15 \pm -0.02$	—
T-astigmatism	$+0.03 \pm -0.01$	$+0.03 \pm -0.01$	—
X-coma	-0.05 ± -0.01	-0.07 ± -0.01	—
Y-coma	$+0.06 \pm -0.01$	$+0.06 \pm -0.01$	—
RSS sum	0.14	0.17	0.15 ± -0.02

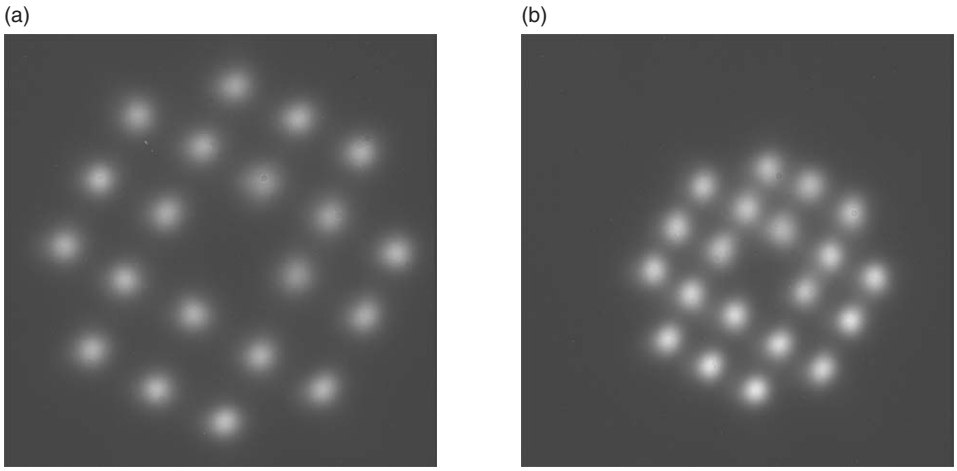

Fig. 6. Coudé images of starlight as seen through the Hartman mask at defocus positions of (a) 0.97 m and (b) 0.64 m.

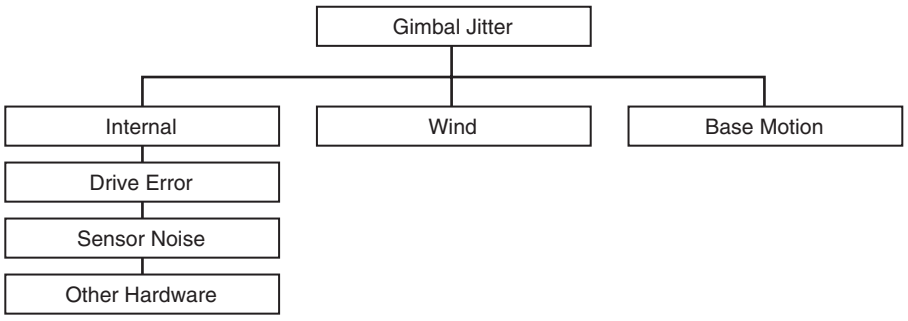

Fig. 7. Telescope jitter budget.

and the telescope pier vibration is also low frequency. However, it can exhibit a narrowband character if it is amplified by resonant modes in the support pier. Predicting the influence of wind is difficult. Clearly, the mean wind speed and gusting at the telescope site are important, but the interaction with the telescope dome slit also plays a role in determining the frequency content of the disturbance faced by the telescope control loop. The control system is particularly sensitive to disturbances with strong frequency content near the feedback loop bandwidth. Data taken at the Table Mountain Facility on the OCTL telescope show that the internal sources and the base vibration contribute little to the telescope jitter during operation.

The control loop architecture for both telescope axes is shown in Fig. 8. The time optimal trajectory and feed-forward controls provide rapid axis positioning but do not compensate for the effects of wind. The digital compensation control loop consisting of the integral control law and the state estimator has a 1-kHz update rate. The power amplifier contains a 400-Hz analog filter to control the digital converter and telescope drive noise. The feedback loop to compensate for wind effects consists of the amplifier and motor, the telescope structure, and the digital compensation control loop. The feedback loop bandwidth is determined by the dynamics of these components.

The control system as set up at the factory was not tuned to compensate for winds at TMF, and initial field test results with factory settings gave poor results, as expected. The disturbance rejection of a simple feedback loop varies as the loop bandwidth (defined as the 0-dB crossover of the open-loop response) squared, and increasing the loop bandwidth reduces the wind-induced gimbal jitter. Yet, increasing loop bandwidth for large structures such as the OCTL telescope is not a straightforward process. The three primary challenges to doing so for the OCTL telescope were as follows:

(1) There are definite torque limits. The available torque for control had to be dynamically split between disturbance rejection and inertial acceleration for fast positioning, in particular for reducing the size of the key hole around zenith. Saturating the control torque would lead the system into non-linear operation and would impact the amount of realizable jitter rejection. As the loop bandwidth is increased, the torque required for wind disturbance rejection also increased.

(2) All structures have flexible body modes that can be excited by the control input. The loop bandwidth is best designed so that it is away from these flexible body modes because of the large changes in the gain and phase associated with these modes. The open-loop response for the OCTL elevation axis is shown in Fig. 9. The elevation axis bandwidth is 6.1 Hz. This reduces the wind sensitivity of the original control system by a factor of four. Adequate stability robustness margins are achieved at 40 deg of phase margin and 6 dB

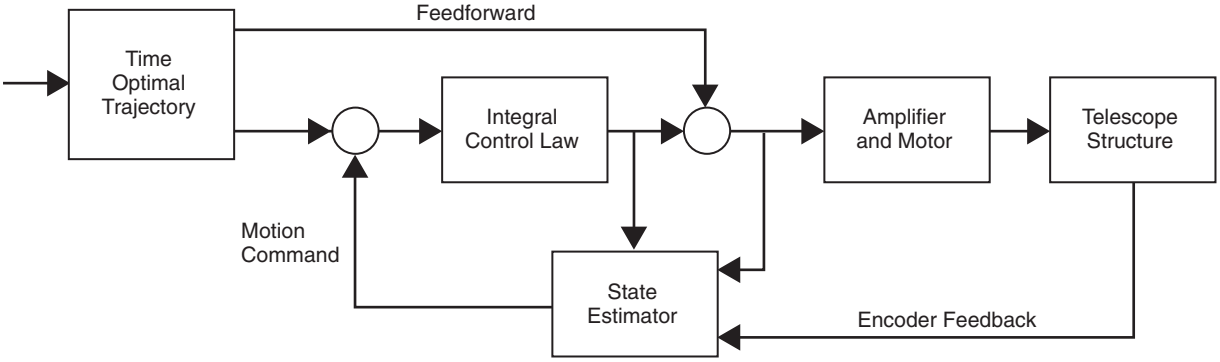

Fig. 8. OCTL telescope control architecture.

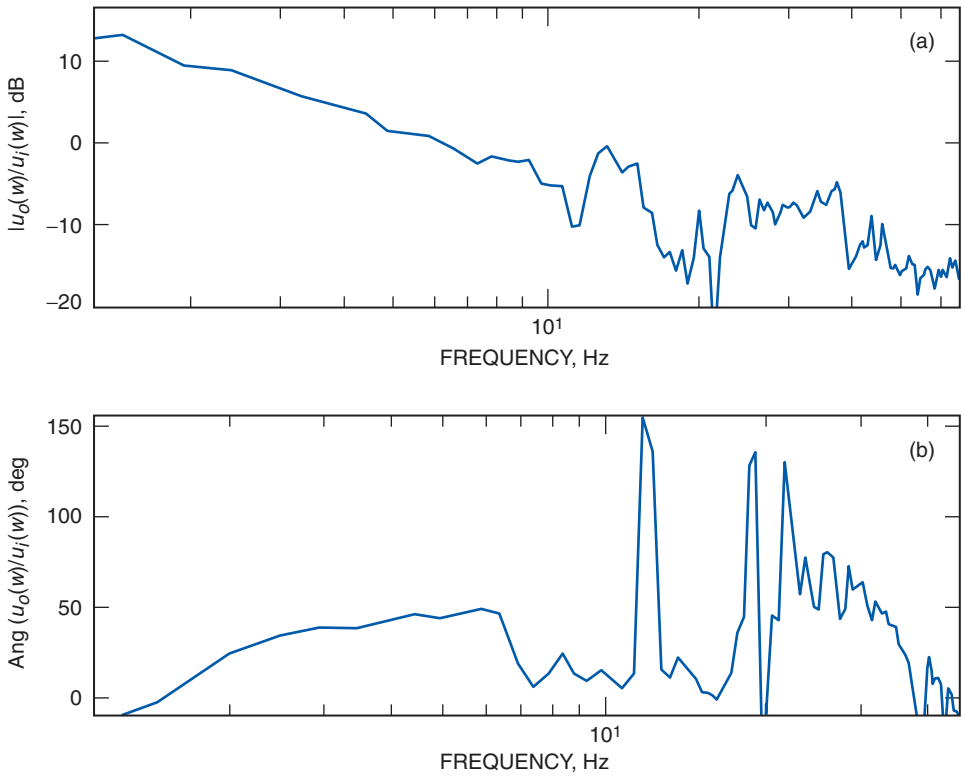

Fig. 9. OCTL telescope elevation axis loop response: (a) amplitude and (b) phase.

of gain margin. The nearby resonant frequency at 13 Hz limits further increases in loop bandwidth. We believe that the azimuth-bearing compliance is the most probable source of this flexible body mode. The elevation motor reaction torque excites the azimuth bearing. The bearing motion is sensed by the encoder and fed back to the loop controller. The telescope has flexible body modes in the structural connections between the secondary mirror/head ring and the gimbal ring (where the motors apply control torque and the encoders measure axis position). These flexible modes are near 45 Hz and do not alter transmission of the wind disturbance, which is limited to 10 Hz. This allows the wind disturbance encountered by the secondary mirror/head ring to be sensed and corrected by the feedback loop.

(3) Typically, sensor noise is most pronounced at high loop bandwidths. The OCTL telescope, however, employs a Brashear-proprietary encoding technology that pushes the sensor-error sources beyond the telescope control bandwidth. These higher-frequency errors then are electronically filtered so that they would have no impact on the telescope performance.

Two different sensors were used to measure the jitter at the microradian level, as required. These were a position encoder (Farrand Inductosyn® 360 cycle) with a noise floor of 0.12 μR rms over a 0.1- to 50-Hz bandwidth and the magneto-hydrodynamic (MHD) sensor (ATA Model ARS-12) that has a noise floor of 0.07 μR rms over a 20- to 1000-Hz bandwidth. The encoder measures the angular deviation of the rotating telescope and is known to be less accurate at high-frequency measurements. The MHD sensor is an inertial device that measures absolute jitter at frequencies above 5 Hz. The different responses of these sensors make the encoder better suited for low-frequency gimbal jitter measurement and the MHD sensor better suited for high-frequency measurement.

Jitter data taken at the TMF are summarized in Table 4. These data were taken with the dome closed to ensure that the test conditions are adequately controlled. Sensor data were sampled at 1 kHz using the real-time computer's data log capability. Given the low-frequency nature of the disturbance sources, it is unlikely that significant jitter exists above 500 Hz and the 1-kHz sampling rate deemed adequate to demonstrate compliance with the specification. Earlier measurements made with the MHD sensor in the 500-Hz to 1-kHz band showed less than 100-nanoradian rms gimbal jitter.

Data were taken with the encoder over the frequency band from 0.1 Hz to 500 Hz and with the MHD sensor from 20 Hz to 500 Hz. Brashear used a proprietary algorithm written in MATLAB to remove encoder artifacts in the data and to divide the encoder data into specified frequency bands. The software also was used to create power spectral density (psd) plots that were integrated over the frequency intervals to calculate the rms gimbal jitter. These results are given in Table 4. The jitter performances specified for the 0.1- to 20-Hz band and for the 20- to 500-Hz band at the given axis rates are shown in columns 2 and 5, respectively, along with the measured performance. Columns 3 and 4 are the results for the sub-bands after the psd was integrated over the specified frequency ranges.

The OCTL telescope is required to operate in 50-km/h (30 mph) winds. Table 5 gives the jitter spectrum in winds up to 40 km/h. Measurements were made using the telescope encoder for both the elevation and azimuth axes. In addition, MHD sensor measurements were made of the elevation axis jitter. Data were collected using the telescope controller data logging feature for time periods of approximately

Table 4. Jitter measurements with the dome closed and air handling fans on.

Data processing	Encoder			MHD
	MATLAB jitter GUI, μR rms			MATLAB jitter GUI, μR rms
	0.1–20 Hz	0.1–50 Hz	20–500 Hz	20–500 Hz
Azimuth				
0 deg/s fans on	0.1	0.2	0.6	0.2
0.007 deg/s fans on	0.2	0.4	0.9	0.2
0.54 deg/s fans on	0.5	0.6	1.0	0.2
2.0 deg/s fans on	1.8	1.8	1.1	0.2
Elevation				
0 deg/s fans on	0.04	0.1	1.7	0.1
0.007 deg/s fans on	0.1	0.3	1.2	0.2
0.54 deg/s fans on	0.8	0.9	1.1	0.2
2.0 deg/s fans on	0.9	1.1	1.3	0.4
Specified performance				
0.007 deg/s required	<10	—	—	<1
0.007 deg/s desired	<2	—	—	<1
0.0071–0.54 deg/s	<10	—	—	<1
0.5–2.0 deg/s	<10	—	—	<1

Table 5. Gimbal jitter in wind (open dome).

Wind, km/h	Elevation angle, deg	Sensor	Jitter, μR rms			
			0.1–5 Hz		5–50 Hz	
			Azimuth	Elevation	Azimuth	Elevation
17–40 direct	45	Encoder	1.6	4.1	2.1	1.1
		MHD	—	6.4	—	1.0
17–40 direct	85	Encoder	0.8	5.0	2.0	1.0
		MHD	—	6.5	—	1.3
25–34 askew (wind at angle to azimuth axis)	85	Encoder	0.8	2.0	3.9	0.9
		MHD	—	5.8	—	0.9

Table 6. The influence of wind on gimbal jitter (0.1–50 Hz) at a tracking rate of 0.007 deg/s.

Wind condition	Azimuth, μR rms	Elevation, μR rms	Comments
17–40 mph wind	2.1	5.1	Elevation result weighted by low-frequency data
Dome closed; no wind	0.3	0.3	—

2 minutes. Expecting that the effect of the wind would have little impact on the massive telescope structure at frequencies beyond 10 Hz, jitter data acquisition was limited to the bandwidth from 0.1 Hz to 50 Hz. The elevation data at the lower frequency range show that the MHD measurements were consistently 50 percent to 100 percent higher than the data for the encoders. This is consistent with our previous experience with this encoder. At the higher frequency range, the encoder and MHD data were within 10 percent with the exception of the 30 percent difference at 85-degree elevation.

In Table 6, we compare key elements of the telescope jitter data at a planetary tracking rate with the dome closed (see Table 4) with that of the dome open during windy conditions (see Table 5). The table shows that the effect of wind is more pronounced on the telescope's elevation axis. This is due in part to the lower inertia (rotating mass) about the elevation axis than about the azimuth axis. In addition to the telescope, the M4 through M6 mirrors and the structure supporting these mirrors in the coudé path rotate around the azimuth axis.

VI. Mount Model and Blind-Pointing Accuracy Performance

The OCTL telescope was constructed to play a significant role in supporting optical communication links for future deep-space missions. Among the requirements for successful links is the ability to blind point to better than 3-arcsec with an all-sky mount model and to better than 2 μrad over a 5-deg segment of sky as based on a local 5-deg field mount calibration. Pointing is dependent on how well an object's position can be determined. The required pointing formats for the telescope are as follows:

(1) Star designate, which allows the telescope to point and track stars from a variety of star catalogs (Hipparcos, FK5, SAO, Tycho) or to point and track a designated right ascension and declination.

(2) Starry Night, a commercial package, allows pointing and tracking of stars, planets, and satellites.

(3) Two-line element sets (TLES) and real-time TLES update the format used for pointing to Earth-orbiting satellites.

(4) Tuned inter-range vector files such as are used by the International Laser Ranging Station Group for precision pointing to Earth-orbiting retro-reflecting satellites.

(5) State vectors, a look-up table, azimuth elevation, and time as used by the Deep Space Network to point to deep-space probes.

(6) Right ascension and declination, for pointing to celestial bodies.

(7) Point mount, a command to point and hold a given pointing direction that is primarily used for horizontal path experiments.

Accurate pointing requires precise knowledge of (1) current time, (2) the geodetic location of the telescope, and (3) mechanical misalignments of the telescope mount. The geodetic location of the OCTL telescope and the updated time inputs to the telescope control system (TCS) are obtained from the Global Positioning System (GPS). A time code generator combined with a GPS receiver mounted on the facility roof provides the TCS with site position to within 10 meters and time to an accuracy within 40 ns. The measured telescope location is 34 deg $22.905' \pm 0.004'$ north latitude and 117 deg $40.962' \pm 0.01'$ west longitude.

Mechanical misalignments in the optical path are calibrated out by developing a mount model for each optical instrument. The Brashear TCS mount model contains 32 coefficients representing errors from geodetic location offsets, mount not level, gravity sag, non-orthogonal axes of rotation, offsets between optical and mechanical axes, bearing wobble, coudé path alignment, and encoder errors. Models are generated by the TCS calibration program based on a set of measured pointing errors acquired from optimally 40 star observations made in the normal and dump telescope positions.

A. All-Sky Blind Pointing Errors

The star calibration procedure was performed over a 6-week period in mid-2004 using a fast-frame CCD camera located at coudé focus. Observations were made using the video output combined with a cross-hair generator, which enabled the operator to center the star within the field of view (FOV) consistently. The number of stars used in each session was chosen to yield results that were statistically representative of the system. This value was entered into the calibration program to automatically select a uniform distribution of stars over the entire sky. After each star was centered about the FOV using the telescope encoder offsets, the program measured the pointing error by computing the angular difference between the expected star position based on the original model (UT date June 17, 2004) and the observed centered position. An rms value for each axis then was calculated from the acquired pointing-error measurements and is tabulated in Table 7.

The preliminary star calibration results show that the all-sky mount model is capable of maintaining accurate pointing well within the blind-pointing specification of 3 arcsec rms over a period of at least 6 weeks. The data also indicate that the elevation-pointing error increased for the last two calibration sessions, which were made after the laser safety system equipment and balancing weights were added to the telescope structure. The increased pointing error suggests an increase in gravity sag or telescope mount flexure due to the additional weight mounted on the telescope. We expect to reduce this contribution with improved telescope balance.

Table 7. OCTL telescope pointing-error results based on star calibrations.

UT date[a,b]	TCS star calibration results		
	Number of observations	Azimuth pointing error, rms, arcsec	Elevation pointing error rms, arcsec
June 17, 2004[D]	99	N/A	N/A
July 2, 2004	51	0.53	0.60
July 29, 2004[D,*]	99	1.09	1.32
July 30, 2004	51	0.74	1.12

[a] A UT date followed by a superscript "D" denotes that the data include observations made at elevation angles >90 deg ("dump" mode).

[b] A UT date followed by a superscript "∗" denotes the addition of equipment to the telescope and rebalancing.

VII. Summary

This article is an interim report on the characterization tests performed at the OCTL telescope to date. We have characterized the OCTL telescope and the atmospheric conditions at TMF, where OCTL site acceptance tests continue to be performed. Several of the key performance parameters of the telescope have been tested. We have identified areas where the telescope performs well within specification (blind pointing accuracy for all-sky star calibration, range of pointing angles, slew rates, key hole, etc.) and areas where it does not (wave-front error and performance under windy conditions). Currently, Brashear is completing several software modifications and upgrades in preparation for a second round of site acceptance testing. These include the Sun-avoidance software for daytime operation and the ephemeris update for real-time adjustments to the telescope pointing when tracking Earth-orbiting satellites.

Acknowledgments

The authors would like to acknowledge the support of Vachik Garkanian and Hossein Hosseini of JPL, who rebalanced the telescope after installing additional instrumentation. The authors would also like to acknowledge the support of Dawn Rucker, Andrew Clarkson, Richard Andre, David Greenwald, and Mike Grumbine of Brashear-LP.

References

[1] K. E. Wilson, J. R. Lesh, K. Araki, and Y. Arimoto, "Overview of the Ground-to-orbit Lasercom Demonstration," *SPIE Free-Space Laser Communication Technologies Proceedings*, vol. 2990, San Jose, California, February 1997.

[2] A. H. Vaughan and D. Mayes, "Optical Metrology of the Optical Communications Telescope Laboratory 1-Meter Telescope by Means of Hartmann Tests Conducted at the Table Mountain Observatory," *The Interplanetary Network Progress Report*, vol. 42-161, Jet Propulsion Laboratory, Pasadena, California, pp. 1–14, May 15, 2005. http://ipnpr/progress_report/42-161/161C.pdf